Electronic Supplementary Material (ESI) for Journal of Materials Chemistry A.

Supporting Information

Distinguishing photo-induced oxygen attack on alkyl chain versus conjugated backbone for alkylthienyl-benzodithiophene (BDTT)-based push-pull polymers

Michael A. Anderson,[a] Anna Hamstra,[b] Bryon W. Larson,[c] and Erin L. Ratcliff *[abd]

[a.] *Department of Materials Science and Engineering, University of Arizona, Tucson, AZ 85721.*
[b.] *Department of Chemistry and Biochemistry, University of Arizona, Tucson, Arizona 85721.*
[c.] *Chemistry and Nanoscience Center, National Renewable Energy Laboratory, Golden, CO 80401.*
[d.] *Department of Chemical and Environmental Engineering, University of Arizona, Tucson, AZ 85721.*

*Correspondence: ratcliff@arizona.edu

Table S1. Details on the polymer names and methods/sources for energy level values.

Push-Pull Name	Other Names	Full Chemical Name	Sources of Redox Level Values
PBDTT-DPP	*NA*	Poly[2,6′-4,8-di(5-ethylhexylthienyl)benzo[1,2-b;3,4-b]dithiophene-alt-5,5'-dibutyloctyl-3,6-bis(5-thiophen-2-yl)pyrrolo[3,4-c]pyrrole-1,4-dione]	CV [1]
PBDTT-EFT	PTB7-Th PCE10 PBDTT-FTTE	Poly[4,8-bis(5-(2-ethylhexyl)thiophen-2-yl)benzo[1,2-b;4,5-b']dithiophene-2,6-diyl-alt-(4-(2-ethylhexyl)-3-fluorothieno[3,4-b]thiophene-)-2-carboxylate-2-6-diyl)]	Optical [2]
PBDTT-FTAZ	J52	Poly[[5,6-difluoro-2-(2-hexyldecyl)-2H-benzotriazole-4,7-diyl]-2,5-thiophenediyl[4,8-bis[5-(2-ethylhexyl)-2-thienyl]benzo[1,2-b:4,5-b']dithiophene-2,6-diyl]-2,5-thiophenediyl]	CV [3]
PBDTT-BDD	PBDB-T PCE12	Poly[(2,6-(4,8-bis(5-(2-ethylhexyl)thiophen-2-yl)-benzo[1,2-b:4,5-b’]dithiophene))-alt-(5,5-(1’,3’-di-2-thienyl-5’,7’-bis(2-ethylhexyl)benzo[1’,2’-c:4’,5’-c’]dithiophene-4,8-dione)]	CV [4]
PBDTT-TPD	PBDTT(EH)-TPD(Oct)	Poly[(5,6-dihydro-5-octyl-4,6-dioxo-4H-thieno[3,4-c]pyrrole-1,3-diyl)[4,8-bis[5-(2-ethylhexyl)-2-thienyl]benzo[1,2-b:4,5-b']dithiophene-2,6-diyl]]	CV (LUMO) & Optical [5]

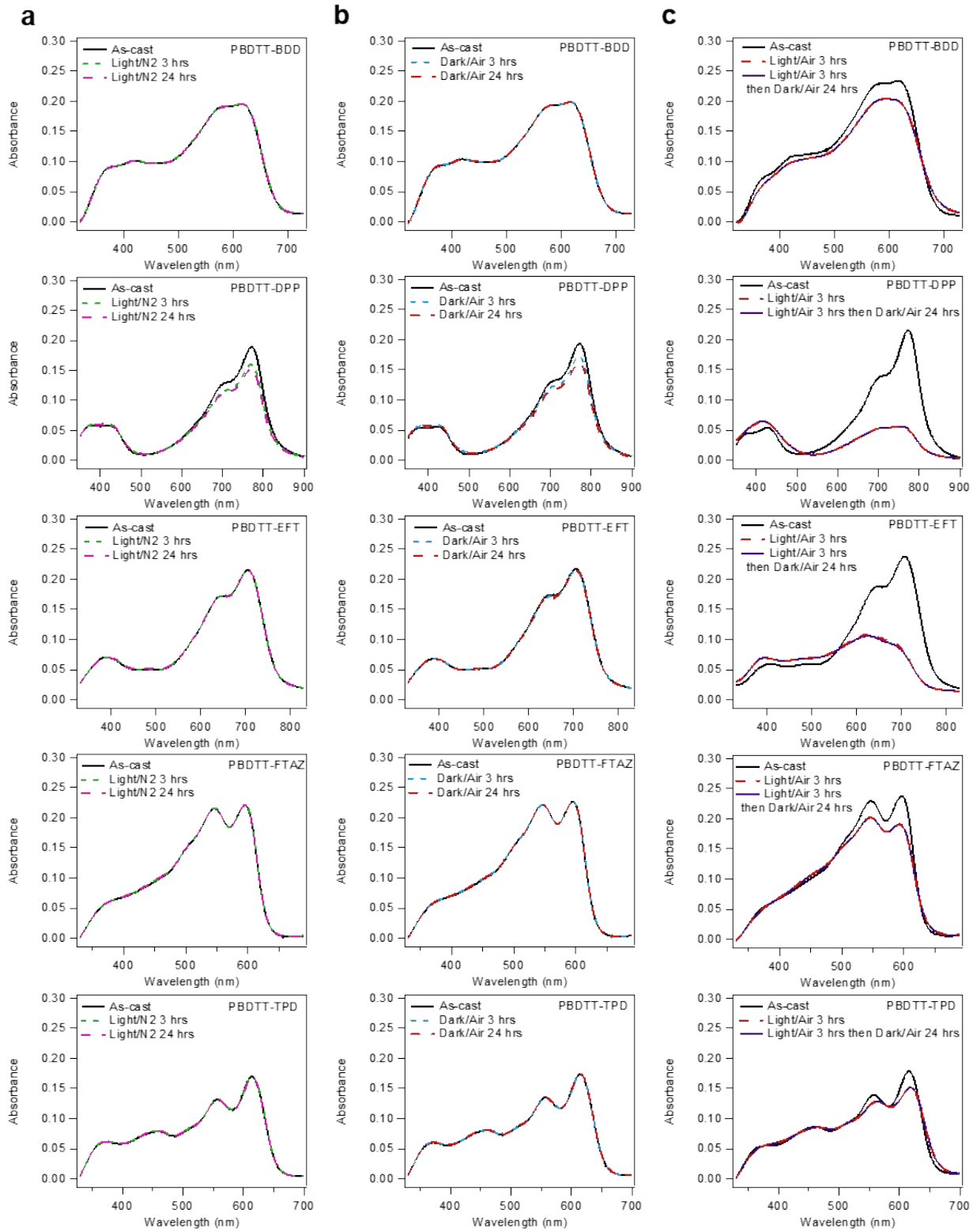

Figure S1. Degradation control experiments. The absorption profiles of the polymers exposed to (a) light in an inert environment, (b) no light in air, and (c) exposed to light in air followed by no light in air. Samples exposed to light in an inert environment or no light in air show negligible changes to the absorption spectra even after 24 hours. The exception is PBDTT-DPP which shows a slight decay in absorption in both cases. For this system, since the decay is most significant in the first 3 hours and occurs regardless of the control (light or environment), the losses may be due to microstructure evolution.

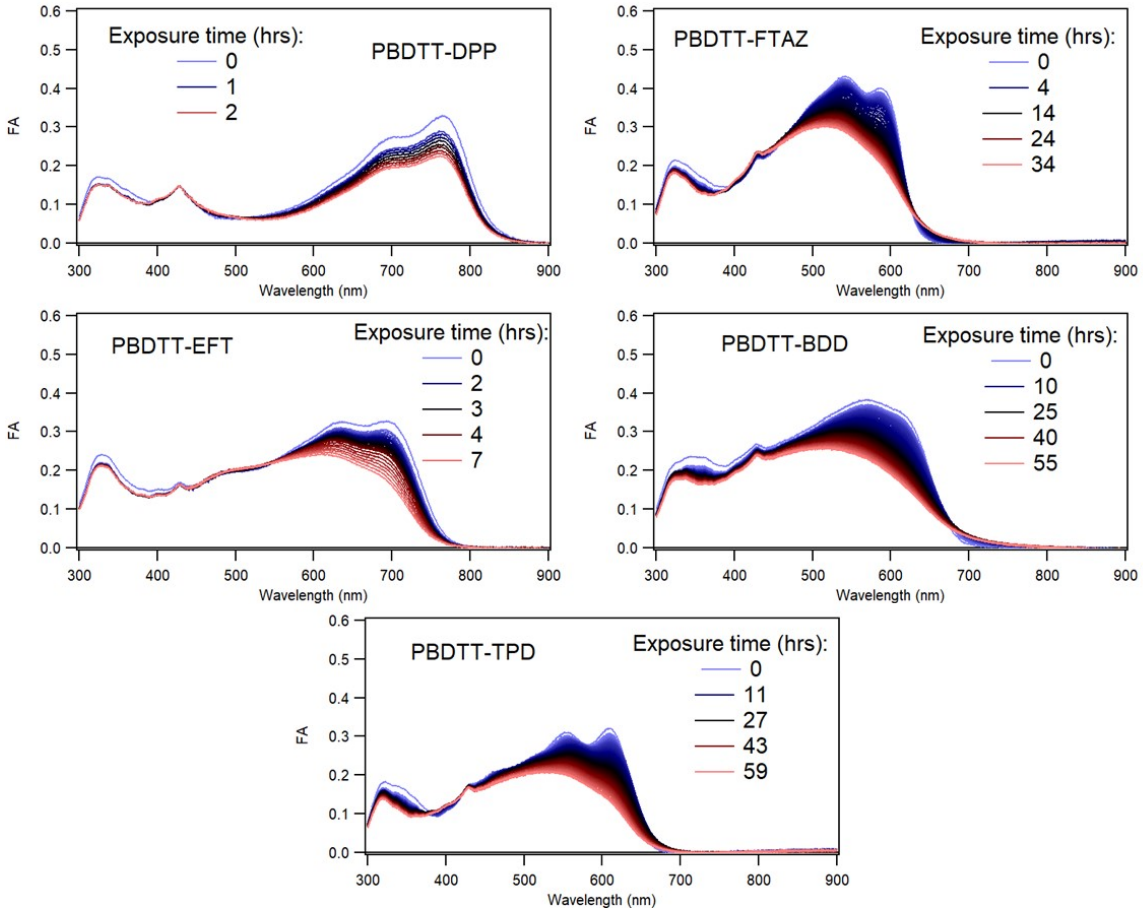

Figure S2. Absorptance spectra of the five PBDTT-pull polymers across the full measurement range (300-900 nm) over the course of photobleaching in ambient. Exposure times to the photobleaching source varied to achieve similar and measurable losses to optical density.

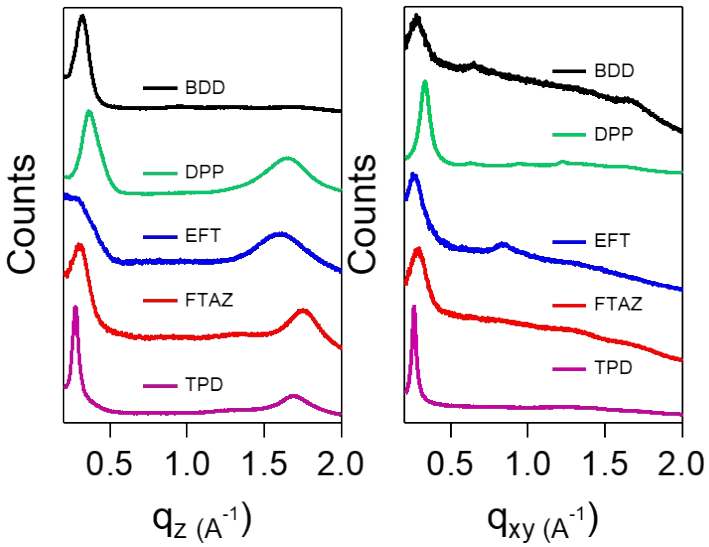

Figure S3. Grazing-Incidence Wide-Angle X-ray Scattering (GIWAXS) one-dimensional intensity vs q_z and q_{xy} profiles for as-cast films of the five PBDTT-pull polymers.

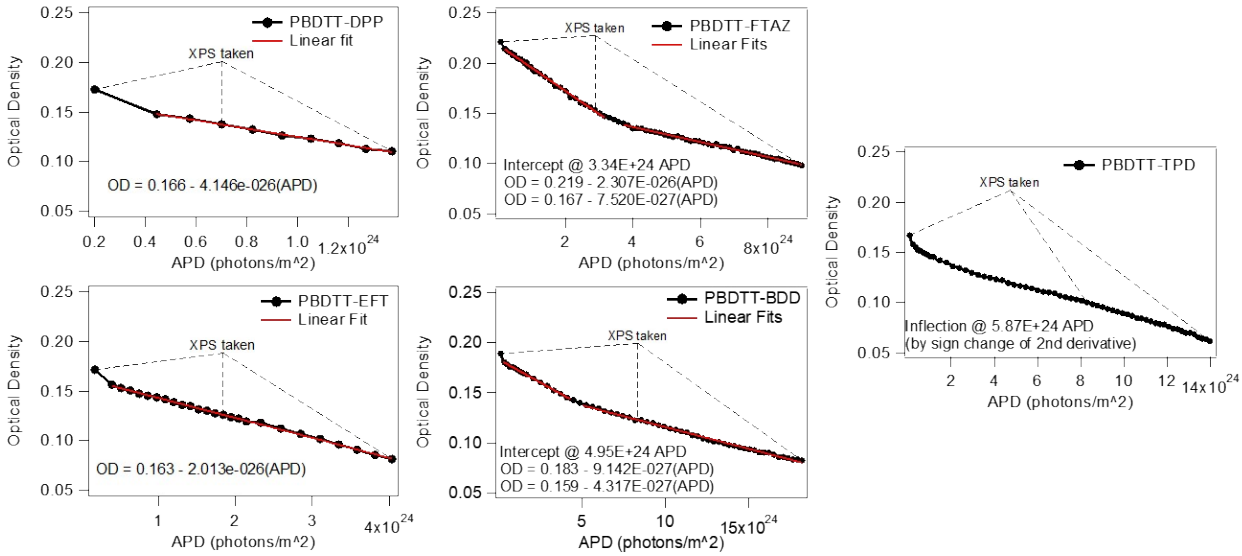

Figure S4. Optical density vs APD line cuts at the 0-0 transitions for each polymer with fits to the linear decay components and identification of the intercepts and inflection points, where applicable.

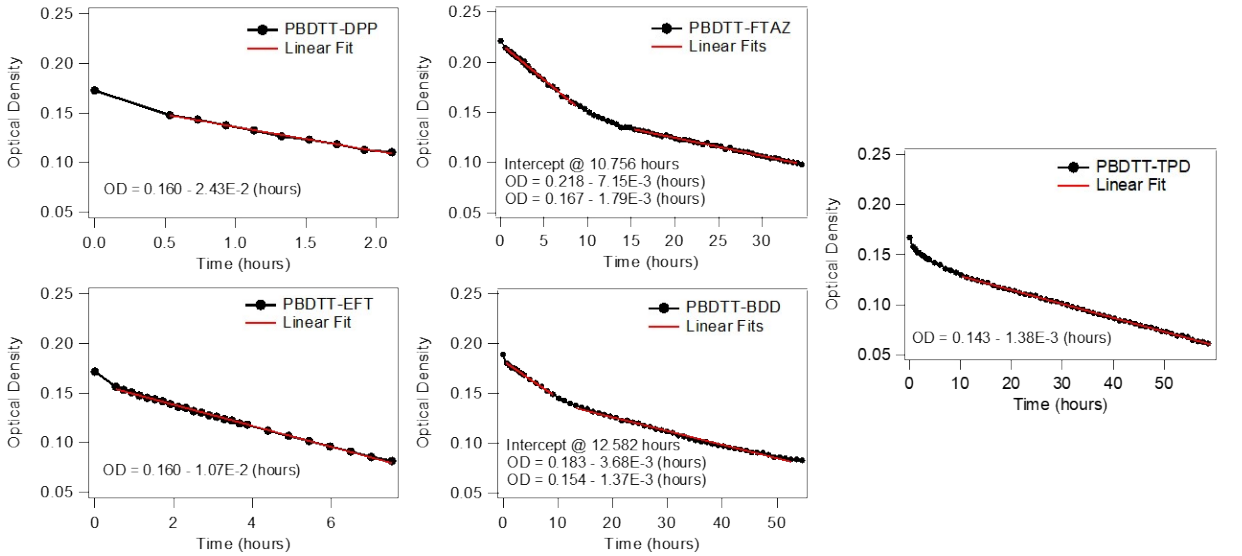

Figure S5. Optical density vs time line cuts at the 0-0 transitions for each polymer with fits to the linear decay components and identification of the intercepts, where applicable.

Table S2. Elemental atomic concentrations as determined by XPS for all 5 polymers after photobleaching exposures of none, low, and high. Exposure times and APDs vary by polymer: exposure information at each setpoint including fractional absorptance (FA) at the 0-0 wavelength of each polymer, accumulated photon dose (APD), and time of exposure. Calculated average oxygen atoms per monomer are included.

XPS Quantifications	Exposure Information				XPS Atomic Concentration (%)					Ave O per
Polymer	Exposure	FA @ 0-0	APD (photons/m^2)	Time (hrs)	C	O	N	S	F	monomer
PBDTT-BDD	None	1.00	0	0.00	89.41	2.11		8.48		2
	Low	0.72	8.35E+24	22.12	84.26	9.25		6.49		8
	High	0.49	1.82E+25	54.58	74.33	18.42		7.25		17
PBDTT-DPP	None	1.00	0	0.00	90.05	1.88	2.20	5.87		2
	Low	0.86	7.00E+23	0.73	87.44	4.40	2.35	5.82		4
	High	0.68	1.37E+24	2.11	85.99	6.26	2.24	5.51		5
PBDTT-EFT	None	1.00	0	0.00	86.74	3.20		8.41	1.65	2
	Low	0.78	1.84E+24	3.09	85.61	4.82		7.89	1.68	3
	High	0.52	4.04E+24	7.54	84.05	6.48		7.90	1.58	4
PBDTT-FTAZ	None	1.00	0	0.00	87.09	0.31	3.56	6.70	2.33	0
	Low	0.74	2.88E+24	9.63	82.98	5.03	3.66	6.22	2.10	4
	High	0.51	9.00E+24	34.55	78.17	9.97	4.01	5.79	2.05	8
PBDTT-TPD	None	1.00	0	0.00	88.53	2.74	1.67	7.06		2
	Low	0.66	8.28E+24	30.93	81.73	9.15	2.34	6.78		5
	High	0.41	1.40E+25	58.67	77.01	13.86	2.75	6.38		9

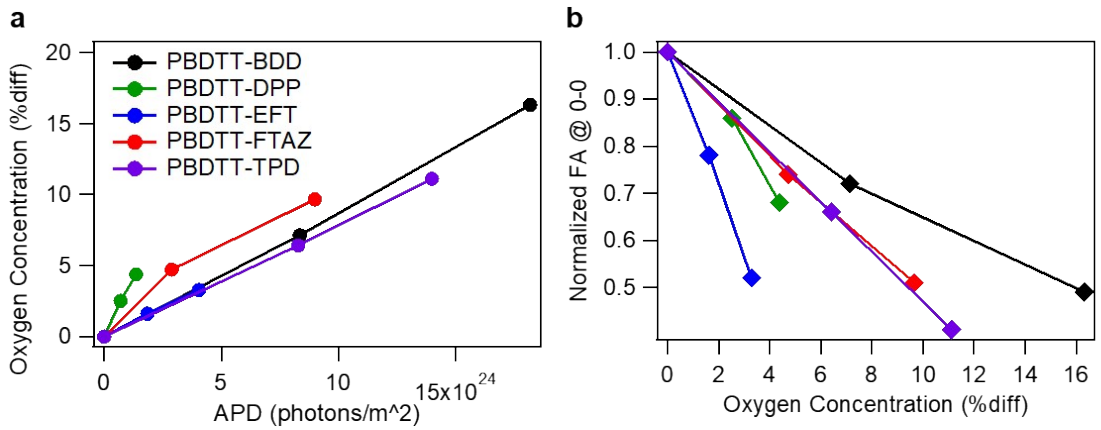

Figure S6. Compiled AIPS and XPS data on the BDTT polymers at the three degradation setpoints of none, low, and high exposures: **a)** Oxygen concentration vs APD and **b)** normalized FA at the 0-0 transition vs oxygen concentration. Oxygen concentrations offset to begin at 0%.

Note S1. Correlation of XPS reporter atom signatures (S 2p) with the chemical structures and degradation pathways.

We note that the first 5 degradation pathways identified in **Figure 3** all result in an oxygen addition a number of bond lengths from a sulfur atom: 3 bond lengths for **reactions 1-3**, 2 for **reaction 4**, and 1 for **reaction 5**. The BEs of S 2p electrons are sensitive to the local bonding environment and the magnitude of the BE shift from a sulfur in a native thiophene, or the degree of perturbation felt though local bonds from the more electronegative oxygen atom, can be correlated to the proximity of added oxygen. In this way, the sulfur atoms act as "proximity detectors" to the site of oxygen addition. The compiled S 2p spectra obtained via XPS for the 5 polymers are shown in **Figure S7** with the difference spectra peaks, obtained by subtracting the degraded spectra from the non-degraded, grouped by BE shifts. The shifts induced by **reactions 1-3**, **4**, and **5** are approximately 0.6, 1.0, and 4.0 eV, respectively. The residual groupings in **Figure S7** motivate the fits of S 2p spectra in the following XPS analysis and allow for determination of the active degradation mechanisms for each polymer.

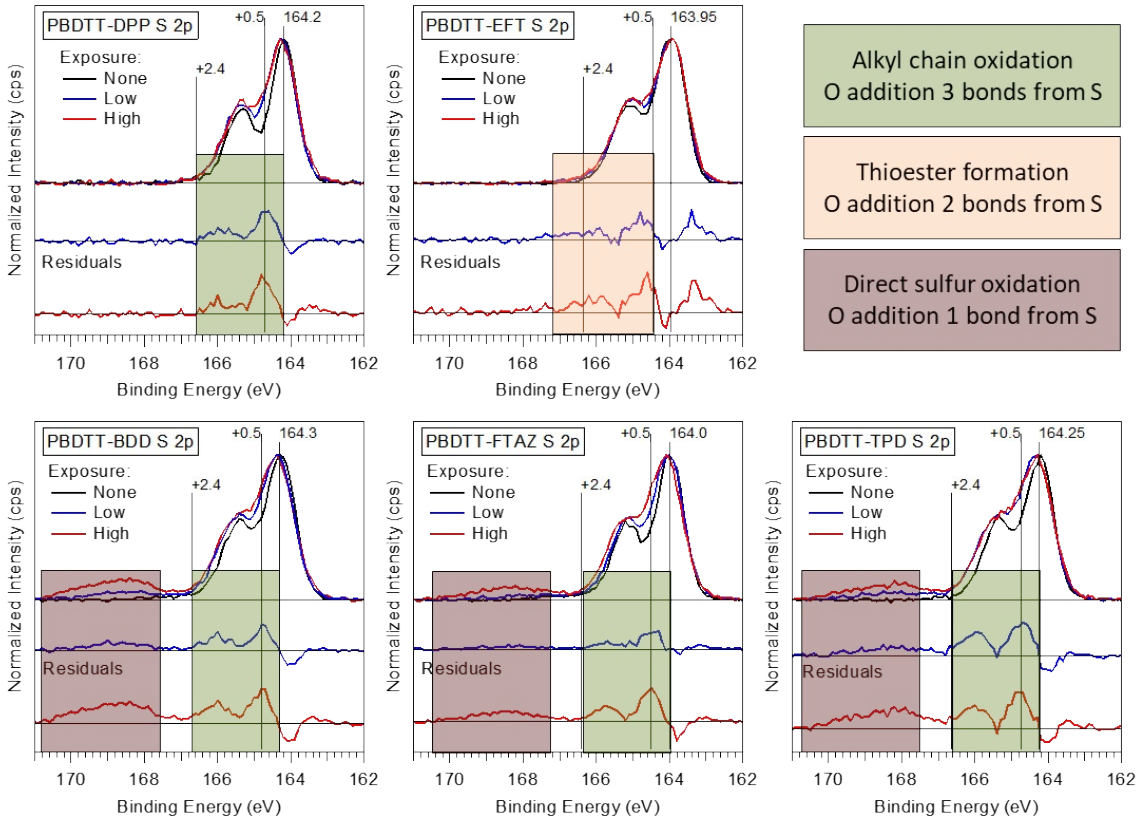

Figure S7. Normalized XPS S 2p spectra for none, low, and high exposures to the photobleaching lightsource and residuals by subtractions of low from none, and high from none. Spectra were shifted in BE to align at the low BE onset. Residual peaks are grouped by the three distinct BE shifts.

Note S2. Chemical pathway steps and support for each of the reactions in Figure 3 of main text.

Reactions 1-3

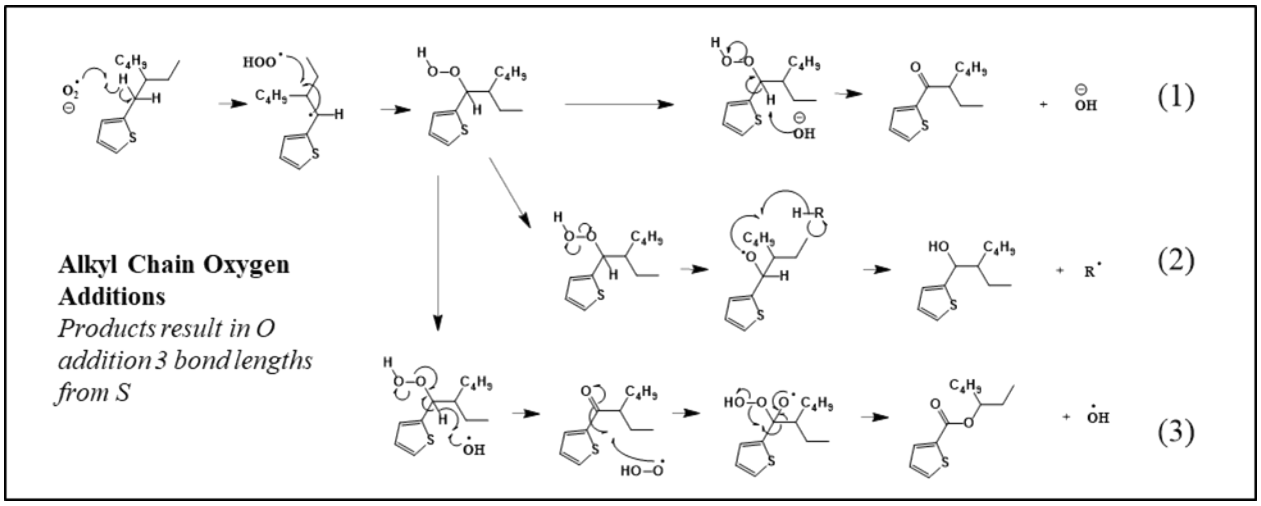

Except from Figure 3. Summary of proposed chemical reactions relevant to the BDTT-based polymers: alkyl chain oxygen additions.

Alkyl chain oxidation is a well-documented photodegradation mechanism for organic semiconductors and the first C-H bonds of side chains have been identified to be the most likely site of attack by oxygen. This has been confirmed by spectroscopic evidence and density functional theory (DFT) calculations for P3HT, [6-8] where the alkyl side chains branch from the 3 position of thiophene, and for PBDTTPD and MDMO-PPV, [9, 10] which have oxyalkyl chains branching from BDT and benzene, respectively. Additionally, Aoyama et al. performed a study on variants of P3HT and found that photodegradation initiates by hydrogen abstraction from the side chains, regardless of side chain structure.[11] While there are demonstrations of increased thermal stability of polymers with alkythienyl-substituted BDT units, [12, 13] to our knowledge, studies specifically investigating the reactivity of sites on BDTT side chains to hydrogen abstraction have yet to be reported. Regardless, due to the structural similarity of an alkylthienyl side chain to a P3HT monomer, despite the alkyl component branching from the 2 position of the thiophene, we construe the C-H bond at the first (alpha) carbon following the thiophene to be the most likely site for alkyl chain oxidation. Initiation at this site can proceed to 3 products as shown by reactions 1-3. Namely, these products are a carbonyl, alcohol, and ester that form through hydroperoxyl radical creation and attachment at the benzylic position followed by (1) a base promoted oxidation, (2) homolytic cleavage of the resulting peroxide and hydrogen abstraction, and (3) Baeyer-Villiger oxidation, respectively. We consider these products the most likely due to the simplicity of the pathway (Occam's Razor), previous XPS, IR, and Raman studies identifying photooxidation-induced functional groups, [6, 9, 14, 15] and verification with our own XPS results. We note that the first step of reaction 3, the Baeyer-Villiger oxidation, is the formation of a carbonyl as in reaction 1. The initiation by either the hydroxyl radical or hydroxide anion are both shown for completeness and are arbitrary assigned. These pathways can proceed through radical propagation to other sites, possibly another alpha carbon on a different alkyl chain. Reactions 1-3 are shown to initiate on the alkyl chain of the BDTT unit, as shared by all 5 polymers in this study, but the mechanism is valid for the side chains of the unique pull units as well.

Reaction 4

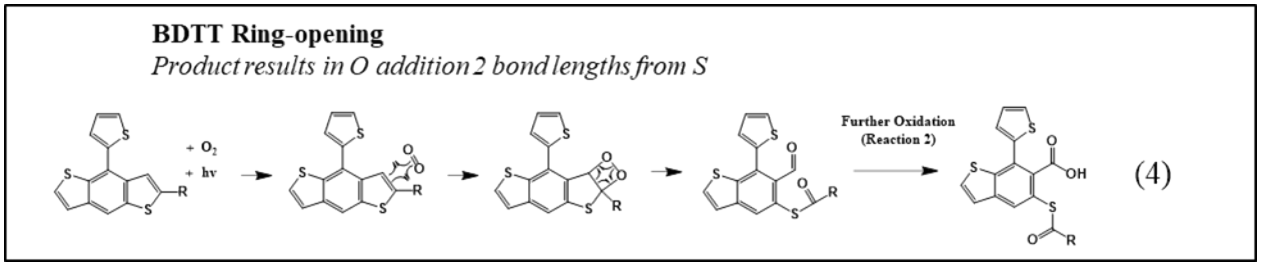

Except from Figure 3. Summary of proposed chemical reactions relevant to the BDTT-based polymers: BDTT ring opening.

Another mechanism of chemical degradation occurs on the conjugated backbone of the BDTT unit as proposed by Kim et al. for PBDTT-EFT. [16] The mechanism differs from reactions 1-3 in that rather than complete electron transfer from the excited polymer to molecular oxygen to form $O_2^{\bullet -}$, there is a charge transfer state initiated by light that causes a [2+2] cycloaddition between a BDTT thiophene and oxygen. This is followed by a retro [2+2] cycloaddition that results in ring opening and the formation of two carbonyls and a carboxylic acid after further oxidation, which are commonly identified products of photooxidation. [8, 9, 14, 16, 17] The thioester formation in particular has been confirmed as a likely product of thiophene oxidation. [18, 19]

Reaction 5

Direct Sulfur Oxidation
Product results in O addition 1 bond length from S

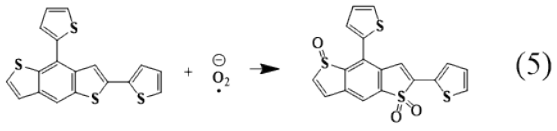

(5)

Except from Figure 3. Summary of proposed chemical reactions relevant to the BDTT-based polymers: direct sulfur oxidation.

The third general mechanism relevant to the chemical degradation of these BDTT polymers is sulfur oxidation. There is an abundance of spectroscopic evidence for the direct oxidation of sulfur in many thiophene-containing polymers including P3HT, [8, 20 6, 7] PTB7, [14] PDPP4T [21], and PCPDTBT. [17] The arrow-pushing steps of electron transfer between sulfur and reactive oxygen species are not well understood, but in the presence of oxygen and light, thiophene can be oxidized as shown in reaction 5, resulting in either a mono- or di-oxidized sulfur atom. [18, 19, 22] This mechanism has been identified to be more likely to occur on thiophenes that are a part of a larger conjugated system, such as benzodithiophene, than those that are more isolated due to lower energy barriers.[22]

Reactions 6-7

TPD Direct Nitrogen Oxidations
Products result in O addition 1 bond length from N

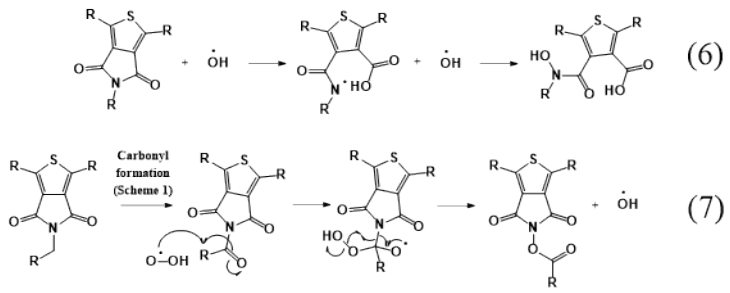

(6)

(7)

Except from Figure 3. Summary of proposed chemical reactions relevant to the BDTT-based polymers: TPD nitrogen oxidations.

A final degradation mechanism, unique to the PBDTT-TPD polymer, is direct oxidation of the nitrogen of the TPD unit as shown in reactions 6-7. Here, there are two routes possible to result in nitrogen oxidation: hydroxyl radical attack (6) or carbonyl formation followed by a Baeyer-Villager-like oxidation (7). In reaction 6, hydroxyl radicals attack the C-N bond of the pyrrole dione causing ring opening and result in a carboxylic acid and directly oxidized nitrogen. The reactive hydroxyl species could originate as products of other active degradation pathways such as the alkyl chain oxygen addition or could be created by homolytic cleavage of hydrogen peroxide. This pathway could proceed regardless of if the TPD alkyl chain has already oxidized. Reaction 7, however, first requires the formation of a carbonyl at the alpha carbon of the alkyl chain, followed by a Baeyer-Villlage-like oxidative cleavage and formation of an ester.

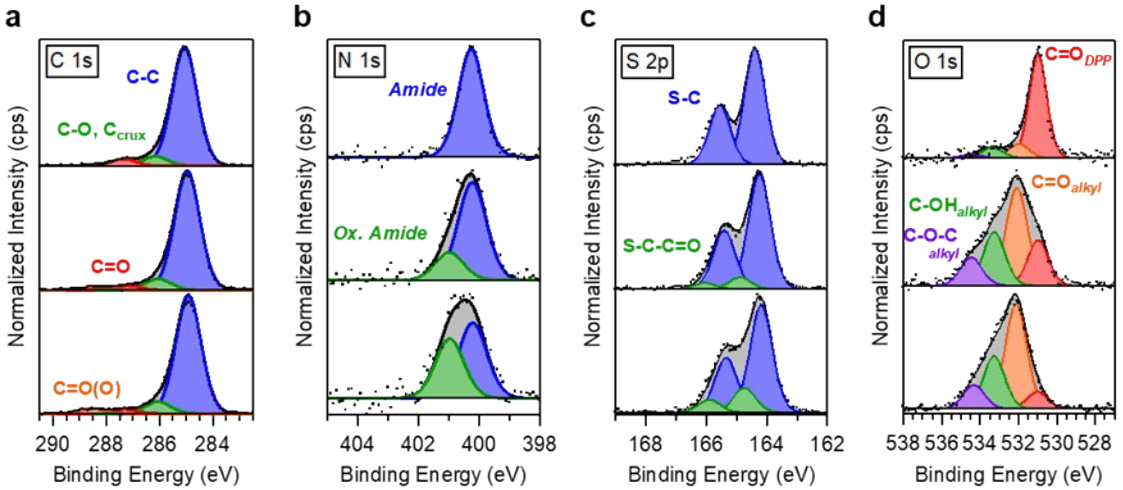

Figure S8. **a)** C 1s, **b)** N 1s, **c)** S 2p, and **d)** O 1s XPS regional spectra for PBDTT-DPP films with photobleaching exposures of none (top), low (middle), and high (bottom), coinciding with APDs of 0, 7.00E23, 1.37E24, and 2, 4, and 5 average oxygen atoms per monomer, respectively.

Table S3. Peak fit parameters including chemical assignment, peak position, full-width half-max, and area percentage for XPS regional spectra of PBDTT-DPP films after APDs of 0, 7.00E23, 1.37E24 on the photobleaching system.

XPS Peak Fits		PBDTT-DPP								
		As-cast			Low			High		
Orbital	Assignment	BE (eV)	FWHM (eV)	Area (%)	BE (eV)	FWHM (eV)	Area (%)	BE (eV)	FWHM (eV)	Area (%)
Carbon 1s	C-C	285.07	1.10	87.7	284.97	1.10	86.1	284.93	1.10	84.3
	C-O, C$_{crux}$	286.18	1.10	7.1	286.06	1.10	8.2	286.07	1.10	8.7
	C=O	287.38	1.10	5.2	287.22	1.10	3.3	287.34	1.10	3.3
	C(=O)O	-	-	-	288.45	1.10	2.5	288.61	1.10	3.8
Oxygen 1s	C=O *DPP*	530.96	1.06	76.4	531.00	1.23	19.4	530.99	1.24	8.2
	C=O *alkyl*	532.00	1.20	11.7	532.10	1.29	44.0	532.14	1.29	53.0
	C-OH *alkyl*	533.34	1.25	9.1	533.28	1.29	24.0	533.28	1.29	26.6
	C-O-C *alkyl*	534.39	1.25	2.7	534.48	1.29	12.6	534.33	1.29	12.1
Nitrogen 1s	Amide	400.26	0.98	100.0	400.24	1.08	77.8	400.21	1.09	56.0
	Ox. Amide	-	-	-	400.99	1.09	22.2	400.96	1.09	44.0
Sulfur 2p	S-C 3/2	164.41	0.80	66.2	164.22	0.85	60.2	164.20	0.85	54.2
	S-C 1/2	165.57	0.80	33.8	165.38	0.85	30.8	165.36	0.85	27.7
	S-C-C=O 3/2	-	-	-	164.87	0.82	5.9	164.75	0.82	12.0
	S-C-C=O 1/2	-	-	-	166.03	0.82	3.0	165.91	0.82	6.1

Note S3. Analysis of XPS regional spectra features arising with the degradation of PBDTT-DPP and correlation to chemical degradation pathways and optical decay behavior.

Figure S8 shows the XPS regional spectra for PBDTT-DPP films after different exposures on the photobleaching system. The corresponding fit parameters including chemical assignment, peak position, full-width half-max, and area percentage are given in **Table S3**. As shown in **Figure S8a**, 84-88% of the total C 1s signal makes up the primary peak (blue) that corresponds to sp^2 and sp^3 hybridized carbon atoms. The rest of the signal towards higher binding energies (BE) is assigned to the carbon atoms bonded in increasing order to oxygen (green, red, orange), aside from some contribution of carbon atoms in crux positions of the BDTT and DPP components. With increasing exposure (top to bottom), an increase in the relative contributions of the higher BE peaks, including the arrival of a peak assigned to a carbon species holding both a single and double bond to oxygen (C=O(O)), is observed.[21, 23] This is consistent with the increases in oxygen content due to photooxidation as described by **reactions 1-4**. The N 1s spectra (**Figure S8b**) has a primary feature (blue) due to the native amide in the DPP component. A higher binding energy component (green) arises with exposure that makes up 44% of the

signal for the highly-exposed sample. To note, this BE shift of c.a. 0.7 eV is consistent with a hemi-aminal, or oxidation of the carbon atom adjacent to the nitrogen, and not direct oxidation of the nitrogen atom itself which has been shown to result in a larger BE shift (c.a. 2 eV). [21, 24, 25] This hemi-aminal formation indicates an alkyl chain oxygen addition occurring on the side chains of the DPP component, while the lack of direct nitrogen oxidation indicates that the DPP skeleton remains intact. The S 2p spectra in **Figure S8c** is also indicative of alkyl chain oxygen addition but on the BDTT unit. The primary features (blue) that corresponds to spin-orbit coupled electrons from sulfur atoms in thiophene are joined throughout exposure by new sulfur species (orange) shifted to higher BE by c.a. 0.6 eV. This shift is consistent with a perturbation to a branching thiophene's sulfur atom by added oxygen 3 bond lengths away on the alkyl chain. Further, no thioester or directly oxidized sulfur species are detected in the exposed S 2p spectra, ruling out significant formation of products by **reactions 4** or **5**. The O 1s spectra (**Figure S8d**) support these conclusions with evidence of the formation of the oxygen products (carbonyls, alcohols, esters). Comprehensive analysis of the regional spectra has narrowed the likely degradation mechanisms of PBDTT-DPP to alkyl chain oxygen addition at the alpha carbon of side chains on both the BDTT and DPP units. Further, the O 1s spectra give insight into the relative amounts of the oxygen products formed at these sites. We differentiate and resolve in BE the XPS oxygen signals of a native polymer carbonyl (red) from an alkyl chain carbonyl (orange), as the former is a component of the conjugated backbone and thereby highly influenced by molecular orbitals while the latter on the periphery of that system.

End of Note S3.

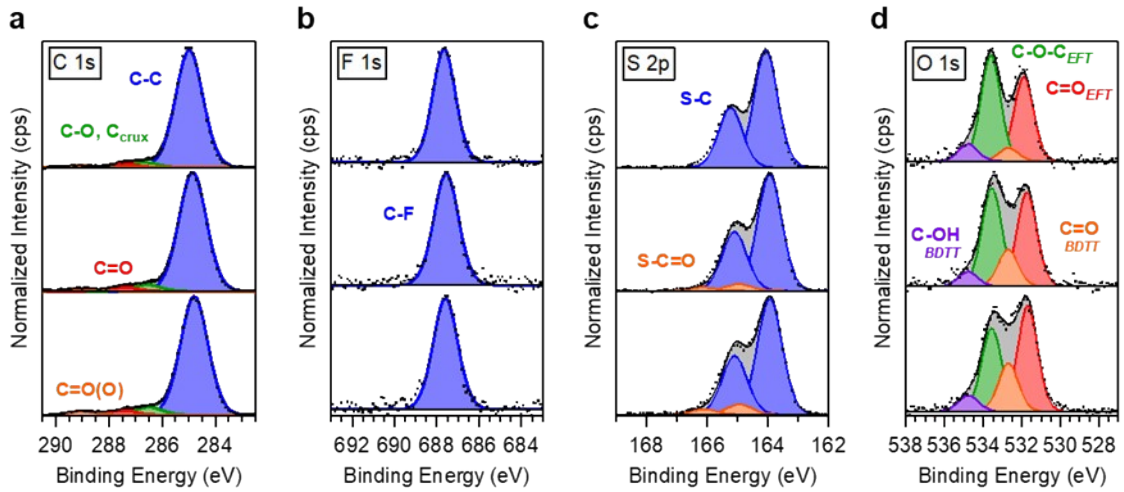

Figure S9. **a)** C 1s, **b)** F 1s, **c)** S 2p, and **d)** O 1s XPS regional spectra for PBDTT-EFT films with photobleaching exposures of none (top), low (middle), and high (bottom), coinciding with APDs of 0, 1.84E24, and 4.04E24 and 2, 3, and 4 average oxygen atoms per monomer, respectively.

Table S4. Peak fit parameters including chemical assignment, peak position, full-width half-max, and area percentage for XPS regional spectra of PBDTT-EFT films after APDs of 0, 1.84E24, and 4.04E24 on the photobleaching system.

XPS Peak Fits		PBDTT-EFT								
		As-cast			Low			High		
Orbital	Assignment	BE (eV)	FWHM (eV)	Area (%)	BE (eV)	FWHM (eV)	Area (%)	BE (eV)	FWHM (eV)	Area (%)
Carbon 1s	C-C	285.00	1.20	91.4	284.87	1.20	89.7	284.80	1.20	87.5
	C-O, C_{cnux}	286.70	1.20	4.0	286.59	1.20	5.0	286.50	1.20	5.9
	C=O	287.47	1.20	2.9	287.44	1.20	3.1	287.48	1.20	3.4
	C(=O)O	289.10	1.20	1.6	289.06	1.20	2.2	289.02	1.20	3.1
Oxygen 1s	C=O *EFT*	531.91	1.16	38.3	531.74	1.20	38.6	531.70	1.20	41.6
	C=O *BDTT*	532.71	1.16	5.9	532.71	1.20	15.1	532.70	1.20	19.0
	C-O-C *EFT*	533.63	1.16	48.0	533.55	1.20	40.3	533.57	1.20	32.9
	C-OH *BDTT*	534.79	1.16	7.7	534.79	1.20	6.0	534.77	1.20	6.5
Flourine 1s	C-F	687.66	1.25	100.0	687.58	1.36	100.0	687.58	1.35	100.0
Sulfur 2p	S-C 3/2	164.07	0.91	66.2	163.94	0.94	62.4	163.96	0.95	60.8
	S-C 1/2	165.23	0.91	33.8	165.10	0.94	31.9	165.12	0.95	31.0
	S-C=O 3/2	-	-	-	164.95	0.96	3.7	164.94	0.96	5.4
	S-C=O 1/2	-	-	-	166.11	0.96	1.9	166.10	0.96	2.8

Note S4. Analysis of XPS regional spectra features arising with the degradation of PBDTT-EFT and correlation to chemical degradation pathways and optical decay behavior.

Figure S9 shows the XPS regional spectra for PBDTT-EFT films after none, low, and high exposures on the photobleaching system. The corresponding fit parameters including chemical assignment, peak position, full-width half-max, and area percentage are given in **Table S4**. We observe the expected increase in oxidized carbon atoms with exposure (**Figure S9a**) but the F 1s core level in **Figure S9b** is unaffected. In contrast to PBDTT-DPP, we do not observe the c.a. 0.6 eV shift of S 2p peaks expected for BDTT unit alkyl chain oxygen addition. We also note that the EFT alkyl chain already has a native ester, eliminating that site for **reactions 1-3**, although oxygen addition at a carbon atom further down the chain could occur. However, in **Figure S9c**, a new species of sulfur (orange) arises with exposure shifted from the native thiophene by c.a. 1.0 eV, evident of oxygen addition 2 bonds from sulfur. Combined with the lack of directly oxidized sulfur species ruling out **reaction 5** products, the dominating degradation pathway is likely **reaction 4**: thioester and carboxylic acid formation via ring opening at the benzo-adjacent thiophene of the BDTT unit. This is in agreement with Kim et al. who proposed the BDTT ring opening pathway for PBDTT-EFT, [16] and with Löhrer et al. who identified the most sensitive reaction site of the polymer to be the conjugated backbone.[26] As shown in **reaction 4**, the initiation of this pathway is via a charge transfer state between the polymer and molecular oxygen that does not result in a mobile radical oxygen species. Instead, the reaction is localized to the conjugated system where the photoelectron is highly distributed. Therefore, it is consistent that a material dominated by this process does not also significantly undergo any of the other degradation pathways since they all require a reactive species to migrate to initiation sites. The O 1s spectra (**Figure S9d**) agrees with the products as the signals from thioester and carboxylic acid oxygen atoms formed on the BDTT unit (orange and purple) increase relative to the native ester oxygen atoms (red and green) on the EFT unit with exposure.

End of Note S4.

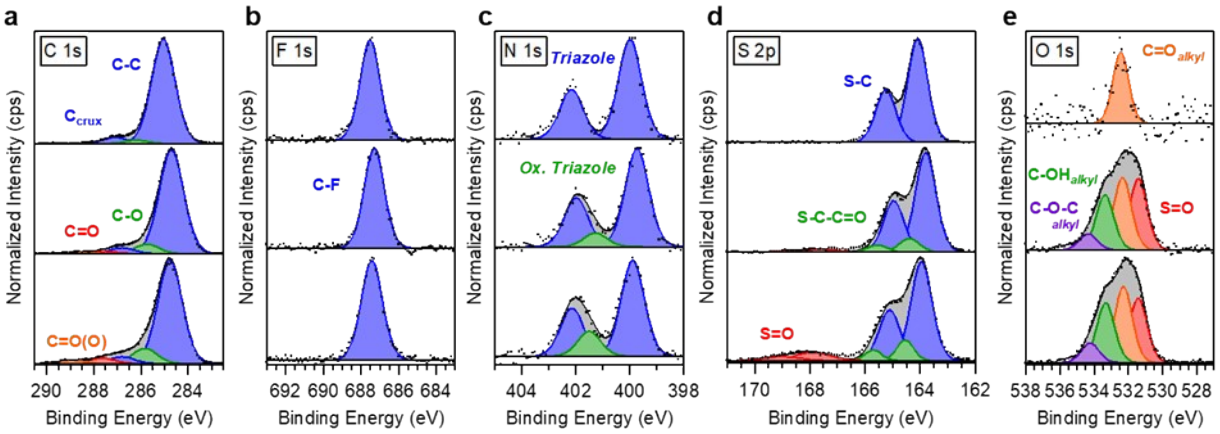

Figure S10. **a)** C 1s, **b)** F 1s, **c)** N 1s, **d)** S 2p, and **e)** O 1s XPS regional spectra for PBDTT-FTAZ films with photobleaching exposures of none (top), low (middle), and high (bottom), coinciding with APDs of 0, 2.88E24, and 9.00E24 and 0, 4, and 8 average oxygen atoms per monomer, respectively.

Table S5. Peak fit parameters including chemical assignment, peak position, full-width half-max, and area percentage for XPS regional spectra of PBDTT-FTAZ films after APDs of 0, 2.88E24, and 9.00E24 on the photobleaching system.

XPS Peak Fits		PBDTT-FTAZ								
		As-cast			Low			High		
Orbital	Assignment	BE (eV)	FWHM (eV)	Area (%)	BE (eV)	FWHM (eV)	Area (%)	BE (eV)	FWHM (eV)	Area (%)
Carbon 1s	C-C	285.07	1.16	91.3	284.72	1.20	83.9	284.77	1.20	76.6
	C-O	286.17	1.20	3.0	285.76	1.20	7.8	285.85	1.20	11.4
	C_{crux}	287.07	1.20	5.7	286.81	1.20	4.9	286.80	1.20	5.3
	C=O	-	-	-	287.50	1.20	1.9	287.64	1.20	4.2
	C(=O)O	-	-	-	288.61	1.20	1.5	288.96	1.20	2.5
Oxygen 1s	S=O	-	-	-	531.43	1.20	33.1	531.44	1.20	29.3
	C=O *alkyl*	532.44	1.08	100.0	532.36	1.20	33.8	532.31	1.20	34.5
	C-OH *alkyl*	-	-	-	533.39	1.20	25.6	533.34	1.20	27.2
	C-O-C *alkyl*	-	-	-	534.36	1.20	7.4	534.25	1.20	8.9
Nitrogen 1s	Triazole (2)	400.02	1.00	66.7	399.76	1.01	61.0	399.92	0.99	56.8
	Ox. Triazole	-	-	-	401.26	1.01	8.5	401.53	1.00	14.8
	Triazole (1)	402.19	1.00	33.3	402.00	1.00	30.5	402.17	0.99	28.4
Flourine 1s	C-F	687.52	1.23	100.0	687.31	1.25	100.0	687.43	1.31	100.0
Sulfur 2p	S-C 3/2	164.08	0.84	66.2	163.80	0.86	55.9	163.98	0.88	50.9
	S-C 1/2	165.24	0.84	33.8	164.96	0.86	28.6	165.14	0.88	25.9
	S-C=O 3/2	-	-	-	164.40	0.84	7.5	164.55	0.68	8.3
	S-C=O 1/2	-	-	-	165.56	0.84	3.9	165.71	0.68	4.2
	S=O 3/2	-	-	-	167.65	1.42	2.8	167.90	1.49	7.0
	S=O 1/2	-	-	-	168.81	1.42	1.4	169.06	1.49	3.6

Note S5. Analysis of XPS regional spectra features arising with the degradation of PBDTT-FTAZ and correlation to chemical degradation pathways and optical decay behavior.

Figure S10 shows the XPS regional spectra for PBDTT-FTAZ films after none, low, and high exposures on the photobleaching system. The corresponding fit parameters including chemical assignment, peak position, full-width half-max, and area percentage are given in **Table S5**. The anticipated increase with exposure of the high BE C 1s peaks is observed in **Figure S10a** and the F 1s spectra in **b** is unaffected. The N 1s spectra (**Figure S10c**) shows two native peaks in a 2:1 intensity ratio and separated by c.a. 2.2 eV, consistent with the three nitrogen atoms in the triazole where the central

nitrogen is in a distinct bonding environment from the other BE-degenerate two. With exposure, a new peak arises that is c.a. 0.7 eV lower in BE than the central nitrogen and c.a. 1.5 eV higher BE than the flanking pair. Logically, the singular nitrogen would be the most perturbed of the three by an oxygen addition to the alkyl chain, though we note that in this case the effect of an oxygen addition two bond lengths away is to lower the effective BE of the nitrogen atom. It is possible that the new peak is due to direct oxidation of the flanking nitrogen atoms, which would be consistent with BE increases observed for other atoms bonded to oxygen, but that would necessitate either a triazole ring opening pathway or a hetero Diels-Alder reaction. We find both unlikely as the optical absorption decay characteristics for PBDTT-FTAZ do not support a third distinct mechanism and there is a lack of literature precedent. Rather, the unique BE response of the central nitrogen to adjacent oxygen addition may be due to the electronic interaction with the flanking nitrogen atoms. Thus, we attribute the new nitrogen peak to correspond to an oxidized triazole following **reactions 1-3** that accounts for 14.8% of the nitrogen signal, or 44.4% of monomers on the film surface.

The S 2p spectra in **Figure S10d** exhibit two new spin-orbit coupled peak pairs with exposure. At the low exposure point we observe features (green) shifted by c.a. 0.6 eV from native thiophene, consistent with alkyl chain oxygen addition, that comprise 11.4% of the total sulfur signal. From the low to high exposure point, these peaks only exhibit a marginal increase to 12.5% contribution. Also arising with 4.2% contribution at the low exposure point but up to 10.6% by the high point are peaks (red) shifted by c.a. 4.0 eV that correspond to oxidized sulfur following the **reaction 5** pathway. The FWHM of these peaks (**Table S5**) is increased to encompass mono- and di-oxidized species. The species present in the O 1s spectra (**Figure S10e**) agree with formation of alkyl chain and sulfur oxidation products. This evidence points towards two mechanisms responsible for the piecewise linear decay in absorption for PBDTT-FTAZ: 1) alkyl chain oxygen addition on both the BDTT and FTAZ units and 2) direct sulfur oxidation most likely occurring on thiophenes of the conjugated backbone.

End of Note S5.

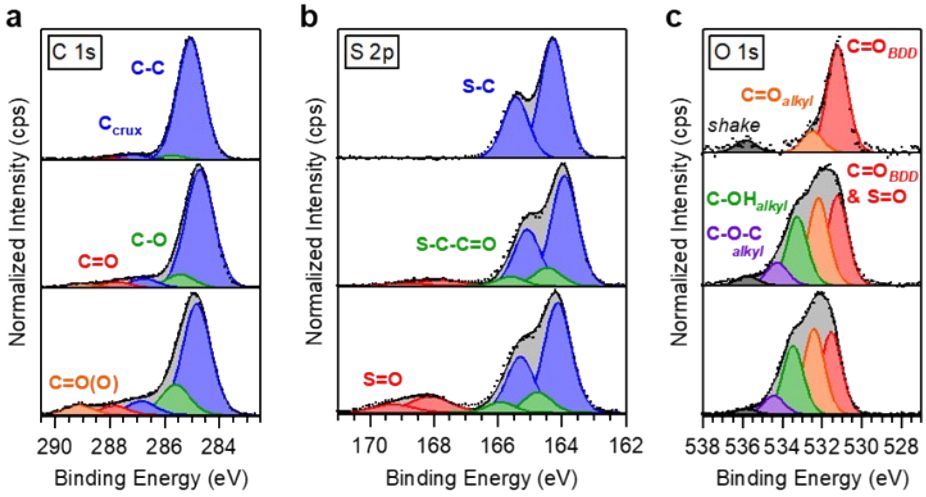

Figure S11. a) C 1s, **b)** S 2p, and **c)** O 1s XPS regional spectra for PBDTT-BDD films with photobleaching exposures of none (top), low (middle), and high (bottom), coinciding with APDs of 0, 8.35E24, and 1.82E25 and 2, 8, and 17 average oxygen atoms per monomer, respectively.

Table S6. Peak fit parameters including chemical assignment, peak position, full-width half-max, and area percentage for XPS regional spectra of PBDTT-BDD films after APDs of 0, 8.35E24, and 1.82E25 on the photobleaching system.

XPS Peak Fits		PBDTT-BDD								
		As-cast			Low			High		
Orbital	Assignment	BE (eV)	FWHM (eV)	Area (%)	BE (eV)	FWHM (eV)	Area (%)	BE (eV)	FWHM (eV)	Area (%)
Carbon 1s	C-C	285.07	1.11	90.3	284.73	1.20	77.9	284.86	1.20	63.7
	C-O	285.75	1.20	3.4	285.45	1.20	8.9	285.64	1.20	17.4
	C_{crux}	287.15	1.20	4.2	286.77	1.20	6.2	286.88	1.20	7.9
	C=O	288.26	1.20	2.0	287.77	1.20	4.2	287.86	1.20	5.2
	C(=O)O	-	-	-	289.06	1.20	2.9	289.16	1.20	5.8
Oxygen 1s	C=O *BDD*, S=O	531.24	1.20	75.9	531.24	1.20	32.3	531.55	1.20	31.5
	C=O *alkyl*	532.50	1.20	15.3	532.20	1.20	31.4	532.42	1.20	32.8
	C-OH *alkyl*	-	-	-	533.27	1.20	24.7	533.48	1.20	26.4
	C-O-C *alkyl*	-	-	-	534.27	1.20	8.3	534.45	1.20	7.2
	shake	535.87	1.20	8.8	535.76	1.20	3.3	535.84	1.20	2.0
Sulfur 2p	S-C 3/2	164.27	0.92	66.2	163.91	0.96	52.5	164.15	0.99	47.0
	S-C 1/2	165.43	0.92	33.8	165.07	0.96	26.8	165.31	0.99	24.0
	S-C-C=O 3/2	-	-	-	164.47	1.00	9.1	164.74	0.99	8.8
	S-C-C=O 1/2	-	-	-	165.63	1.00	4.6	165.90	0.99	4.5
	S=O 3/2	-	-	-	167.80	1.49	4.7	168.12	1.50	10.5
	S=O 1/2	-	-	-	168.96	1.49	2.3	169.28	1.50	5.3

Note S6. Analysis of XPS regional spectra features arising with the degradation of PBDTT-BDD and correlation to chemical degradation pathways and optical decay behavior.

Figure S11 shows the XPS regional spectra for PBDTT-BDD films after none, low, and high exposures on the photobleaching system. The corresponding fit parameters including chemical assignment, peak position, full-width half-max, and area percentage are given in **Table S6**. The chemical structure only consists of carbon, sulfur, and oxygen. The lack of reporter atoms makes localizing degradation pathways difficult but the similarity of the absorption decay characteristics (**Figure S4**) and residual S 2p spectra (**Figure S7**) to PBDTT-FTAZ prompt assignment of the same degradation pathways The average number of oxygen atoms per monomer for PBDTT-BDD (**Table S2**) increases from 2 (native) to 8 (low exposure) to 17 (high). This is a much larger uptake in bonded oxygen than observed for the other polymers. The C 1s spectra in **Figure S11a** reflects this increase as the carbon species bonded to oxygen (green, red, orange), constitute a significant portion (28.4%) of the total signal by the high exposure point. The S 2p spectra (**Figure S11b**) also exhibit significant increases to oxidized products with exposure, corresponding to alkyl chain oxygen addition and direct sulfur oxidation as was for the case of PBDTT-FTAZ. From the low to high exposure points, the sulfur species corresponding to alkyl chain oxidation (**Figure S11b** green) stopped increasing in contribution while the directly oxidized sulfur species (red) increased from 7.0 to 15.8%, likely indicating the saturation of alpha sites for alkyl chain oxygen addition and the subsequent domination of **reaction 5** in the absence of a competing mechanism. In the absence of observed thioester formation, we find the pathways of **reactions 1-3** and **5** to be the most likely for PBDTT-BDD. The species present in the O 1s spectra (**Figure S11c**) agree with formation of alkyl chain and sulfur oxidation products.

End of Note S6.

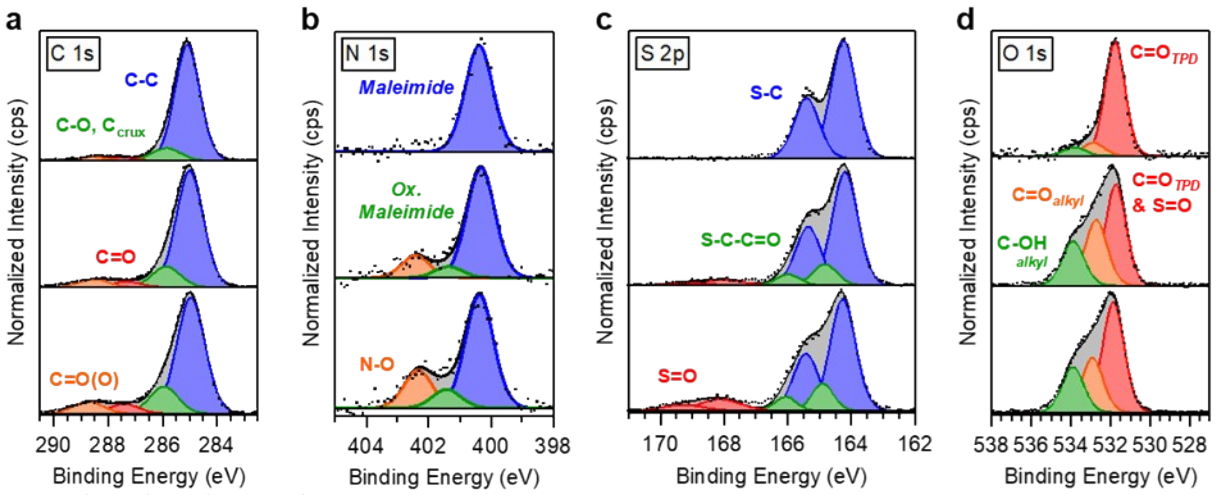

Figure S12. a) C 1s, **b)** N 1s, **c)** S 2p, and **d)** O 1s XPS regional spectra for PBDTT-TPD films with photobleaching exposures of none (top), low (middle), and high (bottom), coinciding with APDs of 0, 8.28E24, and 1.40E25 and 2, 5, and 9 average oxygen atoms per monomer, respectively.

Table S7. Peak fit parameters including chemical assignment, peak position, full-width half-max, and area percentage for XPS regional spectra of PBDTT-TPD films after APDs of 0, 8.28E24, and 1.40E25 on the photobleaching system.

XPS Peak Fits		PBDTT-TPD								
		As-cast			Low			High		
Orbital	Assignment	BE (eV)	FWHM (eV)	Area (%)	BE (eV)	FWHM (eV)	Area (%)	BE (eV)	FWHM (eV)	Area (%)
Carbon 1s	C-C	285.10	1.06	83.6	284.99	1.15	75.9	284.97	1.20	69.6
	C-O	285.88	1.20	10.3	285.88	1.20	14.2	285.96	1.20	16.3
	C=O	287.55	1.20	2.9	287.32	1.25	4.1	287.44	1.29	6.3
	C(=O)O	288.60	1.20	3.2	288.53	1.25	5.9	288.73	1.30	7.8
Oxygen 1s	C=O *TPD* , S=O	531.77	1.17	83.1	531.75	1.21	46.6	531.84	1.27	52.7
	C=O *alkyl*	532.90	1.27	10.3	532.73	1.28	31.9	532.91	1.24	25.5
	C-O *alkyl*	533.85	1.27	6.7	533.89	1.28	21.6	533.88	1.27	21.8
Nitrogen 1s	Maleimide	400.38	1.03	100.0	400.30	1.04	76.8	400.37	1.04	66.7
	Ox. Maleimide	-	-	-	401.35	1.04	7.8	401.43	1.04	11.0
	N-O	-	-	-	402.41	1.04	15.5	402.34	1.04	22.3
Sulfur 2p	S-C 3/2	164.25	0.91	66.2	164.21	0.92	52.8	164.28	0.92	48.2
	S-C 1/2	165.41	0.91	33.8	165.37	0.92	27.0	165.44	0.92	24.6
	S-C-C=O 3/2	-	-	-	164.81	0.87	9.3	164.88	0.77	9.9
	S-C-C=O 1/2	-	-	-	165.97	0.87	4.7	166.04	0.77	5.1
	S=O 3/2	-	-	-	168.051	1.478	4.1	168.150	1.493	8.1
	S=O 1/2	-	-	-	169.211	1.478	2.1	169.310	1.493	4.2

Note S7. Analysis of XPS regional spectra features arising with the degradation of PBDTT-TPD and correlation to chemical degradation pathways and optical decay behavior.

Figure S12 shows the XPS regional spectra for PBDTT-TPD films after none, low, and high exposures on the photobleaching system. The corresponding fit parameters including chemical assignment, peak position, full-width half-max, and area percentage are given in **Table S7**. The 0-0 optical transition decay of PBDTT-TPD (**Figure S4**) does not exhibit clear linear regions. We attribute this to the competition of at least 3 different sets of degradation pathways where the combination of multiple rates and transition points result in nonlinear behavior. As fitting the function to a polynomial removes physical relevance of the coefficients, we suffice to identify the change in curvature to be at 5.87×10^{24} APD, determined as the change in sign of the second derivative in **Figure S4**. The C 1s spectra (**Figure S12a**) contains the usual oxidized species of carbon at higher BE arising with exposure. The S 2p spectra in **Figure S12c** show the same trends as

PBDTT-FTAZ and PBDTT-BDD: an increase in sulfur species (green) corresponding to **reactions 1-3** products (alkyl chain oxygen addition) are initially dominant but reach an apparent saturation between the low and high exposure points; subsequently the **reaction 5** pathway (direct sulfur oxidation) is active, as evidenced by the increase in oxidized sulfur signatures (red). There is also no evidence observed for **reaction 4** thioester formation.

Interestingly, it is the N 1s spectra that elucidates a third chemical degradation mechanism unique to PBDTT-TPD. The primary feature in **Figure S12b** corresponds to the nitrogen in the pyrrole dione of the TPD unit. Upon exposure, we not only observe a new species shifted to higher BE by c.a. 1.0 eV (green), evident of an oxidized pyrrole dione where the alpha carbon of adjacent alkyl chain has been oxidized, but also a new species shifted to higher BE by c.a. 2.0 eV. This latter peak is likley due to directly oxidized nitrogen and prompts assignment of the **reaction 6** pathway in which the pyrrole ring is opened. The other option is since the TPD unit has a non-branched alkyl chain, oxidation could have propagated along it resulting in multiple oxygen atoms within several bond lengths of nitrogen, enhancing the perturbation to BE. We find this unlikely due to the magnitude of the BE shift, the accuracy of the fit using 3 peaks with identical FWHM (rather than 2 peaks with different FWHM that would be motivated with the alternate model), and previous data for a polymer that also exhibited a c.a. 2 eV shifted nitrogen peak but had a branched alkyl chain originating from the amide. [21] As nitrogen species of both oxidized pyrrole diones and directly oxidized nitrogen are present by the low exposure point, it is not clear if the direct nitrogen oxidation pathway proceeds from the alkyl chain oxygen addition or if it initiates independently; the **reaction 6** pathway can proceed from either the native or oxidized TPD. The O 1s spectra in **Figure S12d** gives evidence of native and alkyl chain carbonyls (C=O) and alcohols (C-OH) as oxygen containing products, but the peak indicative of ester (C-O-C) groups observed in the other 4 polymers was absent which is why we assign **reaction 6** and not **7**. The PBDTT-TPD pull unit has two unique characteristics from those of the other polymers: a non-branched side chain and evidence of pyrrole ring opening at the site of chain attachment. It is possible that ester formation on alkyl chains via Baeyer-Villager oxidation has a migratory propensity to the more highly electron-dense pull components of the polymers and in the case of PBDTT-TPD, the TPD unit does not undergo this pathway due to the difference in side chains and/or competition with the pyrrole dione ring opening pathway. Further work would need to be done to validate these conjectures and the broader implications for chemical design.

As in the cases of PBDTT-FTAZ and PBDTT-BDD, the alkyl chain oxygen addition pathways in PBDTT-TPD exhibited initial dominance and eventual saturation, evident by the 14% contribution of S-C-C=O sulfur species to the total signal by the low exposure point and only a 1% increase thereafter. There was no linear slope change to the 0-0 transition decay that could be associated with this saturation, but we previously identified an inflection point to the decay curvature occurring at 5.87×10^{24} APD. Extrapolation of the data in **Table S2** to this APD yields 4 average oxygen atoms per monomer, which corroborates the saturation of the 3 available initiation sites for **reactions 1-3**. This point also occurs at lower APD than the low exposure point, at which we observe a small (6.2%) contribution of **reaction 5** products. The change in curvature at this point is thereby likely due to the termination of alkyl chain oxygen addition and the onset of direct sulfur oxidation. Notably, the N-O nitrogen species (**Figure S12b** orange) constitutes 15.5 and 22.3% of the total nitrogen signal by the low and high exposure points, respectively, indicating that **reaction 6** is active throughout the full photobleaching experiment. Thus, the two regions of distinct curvature apparent in PBDTT-TPD absorption decay are likely the combination of two degradation pathways. The initial optical density decay (positive curvature) being due to alkyl chain oxygen addition and pyrrole ring opening, and the subsequent behavior (negative curvature) is the result of pyrrole ring opening and sulfur oxidation.

End of Note S7.

References

1. L. Dou, J. You, J. Yang, C.-C. Chen, Y. He, S. Murase, T. Moriarty, K. Emery, G. Li and Y. Yang, *Nature Photonics*, 2012, **6**, 180-185.
2. S. Zhang, L. Ye, W. Zhao, D. Liu, H. Yao and J. Hou, *Macromolecules*, 2014, **47**, 4653-4659.
3. Z. Genene, J. Wang, X. Meng, W. Ma, X. Xu, R. Yang, W. Mammo and E. Wang, *Advanced Electronic Materials*, 2016, **2**, 1600084.
4. W. Zhao, D. Qian, S. Zhang, S. Li, O. Inganäs, F. Gao and J. Hou, *Advanced materials*, 2016, **28**, 4734-4739.
5. T. Kim, J.-H. Kim, T. E. Kang, C. Lee, H. Kang, M. Shin, C. Wang, B. Ma, U. Jeong, T.-S. Kim and B. J. Kim, *Nature Communications*, 2015, **6**, 8547.
6. M. Manceau, J. Gaume, A. Rivaton, J.-L. Gardette, G. Monier and L. Bideux, *Thin Solid Films*, 2010, **518**, 7113-7118.
7. M. Manceau, A. Rivaton, J.-L. Gardette, S. Guillerez and N. Lemaître, *Polymer Degradation and Stability*, 2009, **94**, 898-907.
8. H. Hintz, H. J. Egelhaaf, H. Peisert and T. Chassé, *Polym. Degrad. Stab.*, 2010, **95**, 818.

9. A. Tournebize, J. L. Gardette, C. Taviot-Guého, D. Bégué, M. A. Arnaud, C. Dagron-Lartigau, H. Medlej, R. C. Hiorns, S. Beaupré, M. Leclerc and A. Rivaton, *Polym. Degrad. Stab.*, 2015, **112**, 175.
10. S. Chambon, A. Rivaton, J.-L. Gardette and M. Firon, *Journal of Polymer Science Part A: Polymer Chemistry*, 2009, **47**, 6044-6052.
11. Y. Aoyama, T. Yamanari, N. Koumura, H. Tachikawa, M. Nagai and Y. Yoshida, *Polymer Degradation and Stability*, 2013, **98**, 899-903.
12. L. Huo, S. Zhang, X. Guo, F. Xu, Y. Li and J. Hou, *Angewandte Chemie International Edition*, 2011, **50**, 9697-9702.
13. R. Duan, L. Ye, X. Guo, Y. Huang, P. Wang, S. Zhang, J. Zhang, L. Huo and J. Hou, *Macromolecules*, 2012, **45**, 3032-3038.
14. J. Kettle, Z. Ding, M. Horie and G. C. Smith, *Organic Electronics*, 2016, **39**, 222-228.
15. K. E. Watts, T. Nguyen, B. J. Tremolet De Villers, B. Neelamraju, M. A. Anderson, W. A. Braunecker, A. J. Ferguson, R. E. Larsen, B. W. Larson, Z. R. Owczarczyk, J. R. Pfeilsticker, J. E. Pemberton and E. L. Ratcliff, *Journal of Materials Chemistry A*, 2019, **7**, 19984-19995.
16. S. Kim, M. A. M. Rashid, T. Ko, K. Ahn, Y. Shin, S. Nah, M. H. Kim, B. Kim, K. Kwak and M. Cho, *The Journal of Physical Chemistry C*, 2020, **124**, 2762-2770.
17. J. Kettle, H. Waters, Z. Ding, M. Horie and G. C. Smith, *Sol. Energy Mater. Sol. Cells*, 2015, **141**, 139.
18. T. Thiemann, *Journal of Chemical Research*, 2010, **34**, 665-679.
19. M. S. Sharifi, H. Douroudgari and M. Vahedpour, *Scientific reports*, 2021, **11**, 1-20.
20. K. Norrman, M. V. Madsen, S. A. Gevorgyan and F. C. Krebs, *J. Am. Chem. Soc.*, 2010, **132**, 16883.
21. M. A. Anderson, B. W. Larson and E. L. Ratcliff, *ACS Applied Materials & Interfaces*, 2021, **13**, 44641-44655.
22. T. Thiemann, IntechOpen, 2019, DOI: 10.5772/intechopen.79080.
23. Carbon, https://www.thermofisher.com/us/en/home/materials-science/learning-center/periodic-table/non-metal/carbon.html).
24. M. Grzybowski and D. T. Gryko, *Adv. Opt. Mater.*, 2015, **3**, 280.
25. J. Eng, I. A. Hubner, J. Barriocanal, R. L. Opila and D. J. Doren, *J. Appl. Phys.*, 2004, **95**, 1963.
26. F. C. Löhrer, C. Senfter, C. J. Schaffer, J. Schlipf, D. Moseguí González, P. Zhang, S. V. Roth and P. Müller-Buschbaum, *Advanced Photonics Research*, 2020, **1**.